ANISOTROPIC MATERIALS CHARACTERIZATION USING AIR-COUPLED ULTRASOUND

O. I. Lobkis† and D. E. Chimenti
†Center for NDE and
Aero Engrg & Engrg Mechanics Dept
Iowa State University
Ames IA 50011

INTRODUCTION

Ultrasonic materials characterization is widely used to assess both properties and defects of structural components. Recently, the option of gas- or air-coupled ultrasonic testing has become a realistic possibility. In this paper we develop the application of resonant sound transmission methods through ambient air in anisotropic materials with the sound wavevector oriented in a general direction in an anisotropic laminate. Establishing and demontrating the importance of voltage contributions from rays not contained in the incident plane, for sound propagation in a non-symmetry direction, is the major result of this paper.

We proceed by using a rigorous 3-D voltage calculation to isolate the effect of the geometry from the effect of material properties on the observed signals. The voltage consists of contributions from the poles of the reflection coefficient (material properties) and the geometry and saddle point (extrinsic experimental parameters). Estimates of the $\{C_{ij}\}$ for a given sample are calculated iteratively using the measured data to test a maximum likelihood estimator, such as the sum of the squared errors.

Advances in transducer technology have improved signal to noise ratios in air-coupled (A/C) ultrasound. Khuri-Yakub, *et al.* [1] present a design for a highly efficient foil transducer. Suzuki, *et al.* [2] developed a silicon-based electrostatic device, also for robotic imaging applications, which operated in the range of 100 to 200 kHz and included a seven-element array. In more recent developments, transducer design for use at MHz frequencies, utilizing foil transducers has been reported by Wright, *et al.*[3], Anderson, *et al.*[4], Hayward, *et al.*[5], and Haller and Khuri-Yakub [6]. Property measurements have been reported by Hosten, *et al.*[7].

Review of Progress in Quantitative Nondestructive Evaluation, Vol. 16
Edited by D.O. Thompson and D.E. Chimenti, Plenum Press, New York, 1997

Much of the work in air-coupled ultrasonics has been largely qualitative nature, imaging of defects in air-coupled C-scans or approximate estimates of material constants in phase-matched coupling to guided wave modes. Recently, we have demonstrated [8] that, despite the signal-to-noise penalty incurred with air-coupled ultrasonics, the A/C method can be made to yield accurate quantitative measurements of material properties in a variety of materials and material combinations and is especially well suited to the characterization of anisotropic composites. After a brief review of the theoretical calculation leading to the 3-D voltage expression in a two-transducer measurement, we explain the importance of the out-of-incident plane integration for an anisotropic medium in a non-symmetry direction. We also describe the experimental method and analysis; finally, we use these tools to characterize anisotropic plates of composite laminates.

3-D VOLTAGE CALCULATION

In the experimental two transducer arrangement of Fig. 1, the received voltage is a function of both the extrinsic experimental parameters and the intrinsic plate properties, through the plate transmission coefficient. We have shown that the extrinsic parameters can be isolated from the transmission characteristics [9] by modeling the 3-D field of the incident beam at the receiver and accounting for the receiver characteristics by appeal to reciprocity. In Fig. 1 a sound beam from the transmitter falls on the plate at an incident angle α, and the subsequent transmitted field induces a voltage in the receiving transducer. The corresponding spectral integrals, including the effects of both transducers, are

$$\begin{aligned} V(x;\alpha) &= i\kappa a^4 \int_0^{2\pi} \int_0^{\pi/2-i\infty} T(\theta_i,\phi_i) D^T(\gamma) D^R(\gamma) \\ &\quad \times \exp[i\kappa(z_0-d)\cos\theta_i + i\kappa(x_0+x)\sin\theta_i\cos\phi_i]\sin\theta_i\, d\theta_i\, d\phi_i \end{aligned} \tag{1}$$

where z_0 is the total vertical distance between the transducers x is the transducers' separation along the guided wave propagation direction from the symmetrical position x_0 $(= z_0 \tan\alpha)$, κ is the sound wavenumber in air, a is the radius of the transducers, α is the incident angle (measured between the normal to the transducer face and the plate normal), $T(\theta_i, \phi_i, \{C_{ij}^*\})$ is the transmission coefficient (a function of complex viscoelastic properties), $D^{T,R}(\ )$ are the beam directivity functions for the transmitting and receiving transducers, d is the thickness of the plate, and γ is the angle between transmitter acoustical axis and each incident plane-wave direction of propagation (θ_i, ϕ_i) in three dimensions.

An example of the measured (solid curve) combined directivity function $D_T D_R$ and calculated prediction (dashed) is shown in Fig. 2 for a 10-mm diameter foil transducer at 700 kHz. From the figure, the transducer effectively transmits or receives waves in an angular region of about $\pm 3°$. The inset shows schematically the beam diffraction in the incident plane with angular spreading $\Delta\theta$ and spreading in the object plane of $\Delta\phi$. The plate transmission coefficient (TC) has a strong functional dependence on the incident angle θ_i, with the sharp maxima at angles coresponding to Lamb mode excitation. Because of the large acoustic impedance difference between the plate and the air, the range over which $T(\theta_i, \phi_i)$ changes can be much less than the extrinsic beam spread $\Delta\theta$ owing to diffraction.

This means the plate transmission characteristics will select that part of the incident beam angular distribution (which may not be near the central ray at α in

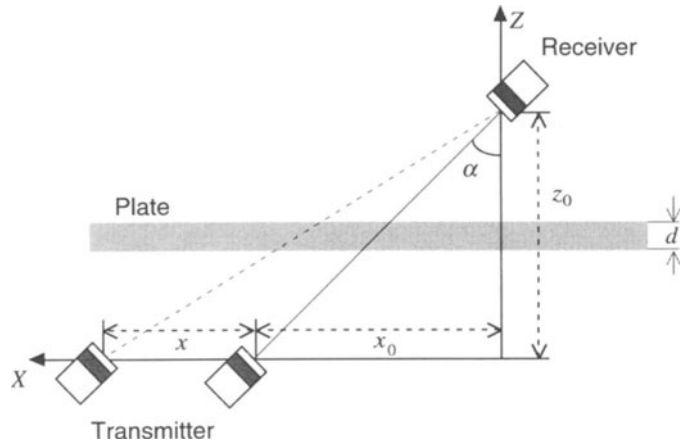

Figure 1. Schematic diagram of the experimental geometry, showing transducer placement and position scanning operation in through transmission.

Fig. 1) to contribute to the output signal. Moreover, the beam diffraction in the plane of a plate can be asymmetrical for anisotropic materials because the effective material constants in that case are functions of the in-plane angle, that is, $C_{ij}(\Delta\phi)$. For strongly anisotropic materials, such as fiber composites, the angular beam spread must be taken into account.

The transform signal $S(\theta;\alpha)$ can be constructed by a coherent summation of signals measured at different x. This coherent sum can be carried out in the form of a Fourier transform, consisting operationally of summing the measured voltage signals, each weighted by the appropriate plane wave whose phase corresponds to that value of x [8]. The result is given by

$$S(\theta;\alpha) = \int_{-\infty}^{\infty} V(x;\alpha)\exp[-i\kappa x\sin\theta]\,dx\,. \tag{2}$$

Then, to compensate for the narrowness of the directivity function, a larger aperture is synthesized by making measurements at several angles and summing them incoherently, $S(\theta) = \sum_\alpha |S(\theta,\alpha)|$, to create a transmission function with a square window aperture. $S(\theta)$ has a close relationship with the magnitude of $T(\theta_i,\phi_i)$. Combining the equations Eq (1) and Eq (2) yields (suppressing a multiplicative factor)

$$S(\theta) = \int_0^{\pi/2-i\infty} [T(\theta_T,\phi_T) + T(\theta_T,-\phi_T)]e^{i\kappa z_0\cos\theta\cos\beta}\,d\beta\,, \tag{3}$$

where $\cos\theta_T = \cos\theta\cos\beta$ and $\tan\phi_T = \sin\beta\cot\theta$ are the angles projected onto the scan axis ($\beta = 0$). The principal signal contribution to $S(\theta)$ in Eq (3) will arise when β is within $(\kappa z_0)^{-1/2}$ of the axis. Only for plane waves, when $\kappa z_0 \to \infty$, does $S(\theta)$ become identical to the plane-wave TC $T(\theta)$ for the xz incident plane. In experiments the difference between $S(\theta)$ and $T(\theta)$ depends on the value κz_0, the plate properties, and its orientation, since they are included in the integrand in Eq (3). Therefore, for anisotropic media there is a substantial difference between the 3-D model result $S(\theta)$ and the plane-wave approximation signal $T(\theta)$. Ignoring this effect will lead to the inference of erroneous material properties from experimental data.

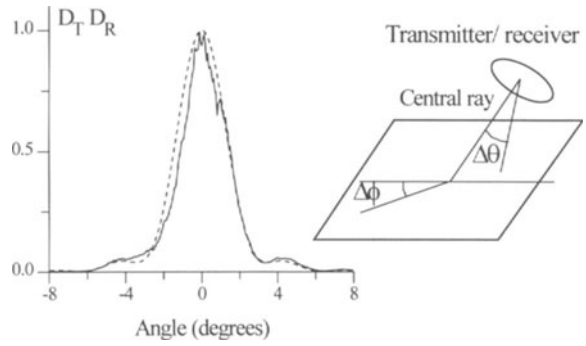

Figure 2. Experimental (solid) and theoretical (dashed) combined directivity function $D_T D_R$ for 10 mm foil transducer at 700 kHz. Inset shows the beam spread angles in and out of the incident xz plane.

RESULTS

For an isotropic plate the material properties do not depend on direction. The TC is a function of the angle θ_T, and only the beam spread in the incident xz plane is important. Experimental and theoretical results for a plexiglas plate are presented in Fig. 3. The solid curve in both graphs is the measurement, the dotted curve in the left-hand graph is the calculated best-fit signal $S(\theta)$, and the dotted curve in the right-hand graph is the TC $T(\theta)$ for the same material parameters. The calculated peak positions, which correspond to the Lamb mode excitation angles, are identical in both curves $S(\theta)$ and $T(\theta)$. For this reason the plane-wave approximation can be reliably used for velocity estimation in isotropic plates, since the peaks positions are determined by these values. At the same time, using this approximation to model material damping gives incorrect results unless the diffraction contribution is taken into account. This is because the widths of the peaks and their amplitudes, features critical to infer damping characteristics, are different for $S(\theta)$ and $T(\theta)$, as seen in right-hand plot in Fig. 3.

For an anisotropic medium with sound propagating along a symmetry direction, such as in a uniaxial laminate along ($\phi = 0°$) or normal ($\phi = 90°$) to the fibers, contributions from $\pm\phi_T$ will be essentially identical because $T(\theta_T, +\phi_T) = T(\theta_T, -\phi_T)$ in Eq (3). The calculated signal $S(\theta)$ is presented for $\phi = 90°$ (left-hand side) and for $\phi = 0°$ (right-hand side) in Fig. 4 where the ϕ_T-dependence of the TC $T(\theta_T, \phi_T)$ near one of the symmetry axes for a uniaxial laminate *is* accounted for (solid curves) and *is not* accounted for (dotted curves). Some small differences in the peak amplitudes can be observed in the left-hand graph when the direction of scanning is perpendicular to the fibers. For the direction of scanning along the fibers the difference between the two curves in the right-hand graph is larger, especially at small incident angles. Two effects contribute to this disparity. First, near the fiber direction the elastic stiffness C_{11} is changing rapidly with angle. Also, at incident angles closer to normal incidence, the wavevector geometry implies that a larger angular range in ϕ_T will contribute to the integral in Eq (3). Near the longitudinal critical angle, in particular, $S(\theta)$ is sensitive to changes in this velocity. The variation in $C_{11}(\phi_T)$ causes the output signal $S(\theta)$ to vary; this may be compared with the case when the on-axis TC $T(\theta_T, \phi_T = 0)$ is the only contribution to the signal calculation in Eq (3).

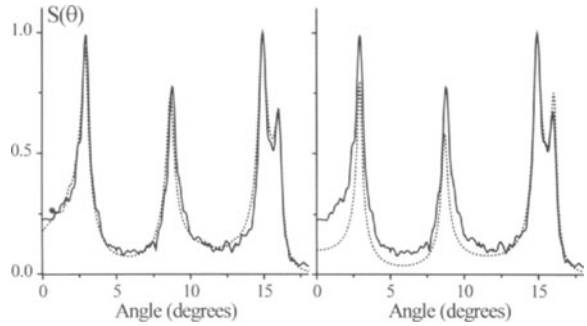

Figure 3. Experimental (solid) and theoretical transmission function $S(\theta)$ (dotted left), and plane-wave transmission coefficient $T(\theta)$ (dotted right), as a function of angle from the normal. The material is a 2.3-mm plexiglas plate measured at 700 kHz.

An example of experimental material characterization is presented in Fig. 5 for a scan normal to the fibers $\phi = 90°$. The 3.6-mm carbon-epoxy plate is measured at 600 kHz (left-hand plot) and 900 kHz (right-hand plot), and the data are compared to a best-fit calculated signal $S(\theta)$ from Eq (3). The inferred values of the viscoelastic constants are $C_{22} = C_{33} = 15.4 - 0.4i$, $C_{23} = 8.1 - 0.2i$, and $C_{44} = 3.7 - 0.1i$. Other material constants have a much weaker influence on the signal for this scan direction and so cannot be reliably reconstructed. For the constants cited above, however, the sensitivity of this method is high enough to discern a 1 or 2% shift in the constants.

For a general scan direction in the uniaxial plate (for example, $\phi = 45°$), the ϕ_T dependence of the TC is a critical factor in obtaining an accurate result, and the calculation must include this contribution. For a general inplane angle the plate properties are not symmetric about the scan direction, and $T(\theta_T, +\phi_T) \neq T(\theta_T, -\phi_T)$ in Eq (3). For the uniaxial composite this effect is especially pronounced. The experimantal signal $S(\theta)$ is presented in Fig. 6 as the solid curve for a 3.6-mm uniaxial carbon-epoxy laminate plate with propagation at $\phi = 45°$. The dashed curve shows the calculated transmission function $S(\theta)$ using approximately determined (without complete solution of the inverse promlem) values for the real and the imaginary parts of the five transversely isotropic material constants C_{ij}. The dotted curve in Fig. 6 is the transmission coefficient $T(\theta)$ calculated for the same C_{ij} values as the signal $S(\theta)$. Both the peak amplitudes and their positions are now different for the functions $S(\theta)$ and $T(\theta)$.

Waves propagating in directions where $\phi > 45°$ ($\phi_T > 0$ in Eq (3)) have different phase velocities from those waves for $\phi_T < 0$. As a result, all these rays have different values of phase at the receiver surface. Coherent summation influences the signal and causes the peaks and their amplitudes to shift from the simple TC calculation. Using only $T(\theta, \phi = 45°)$ is equivalent to calculating the signal without taking into account the phase and the amplitude distributions on the receiver surface, that is, only for incident plane waves. Moreover, the group velocity direction does not coincide with the wavevector. This effect also causes an additional asymmetry in the transmitted wave on the receiver surface. The example in Fig. 6 demonstrates conclusively that only a complete 3-D solution will suffice to model reflected or transmitted signals in a two-transducer geometry, particularly when the sound wave interacts with anisotropic media in an arbitrary direction. To extract either real or imaginary material properties in such a measurement, the full 3-D calculation is an essential tool.

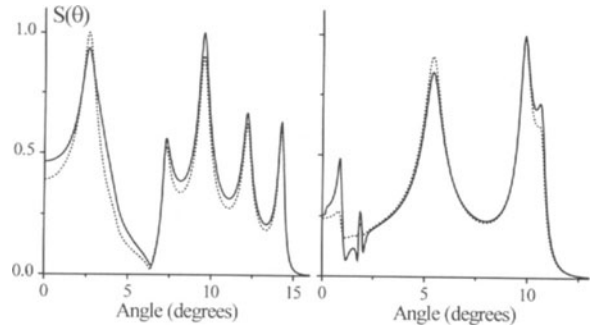

Figure 4. Calculated signal $S(\theta)$ for 3.6 mm uniaxial carbon-epoxy laminate plate with (solid curves) and without (dotted curves) ϕ_T dependence of the transmission coefficient. The scanning direction is perpendicular to the fibers in the left graph and along fibers in right graph.

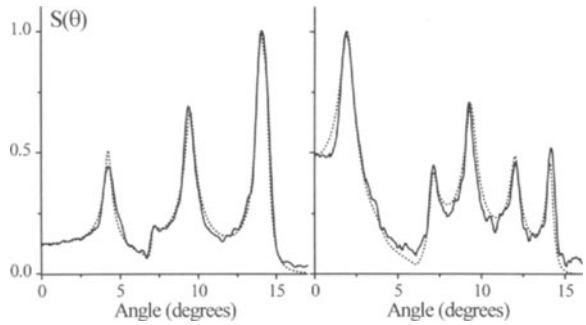

Figure 5. Experimental (solid curves) and theoretical transmission function $S(\theta)$ (dotted curves) for scanning direction perpendicular to the fibers for 3.6-mm carbon-epoxy laminated plate at frequencies of 600 kHz (left-hand plot) and 900 kHz (right-hand plot).

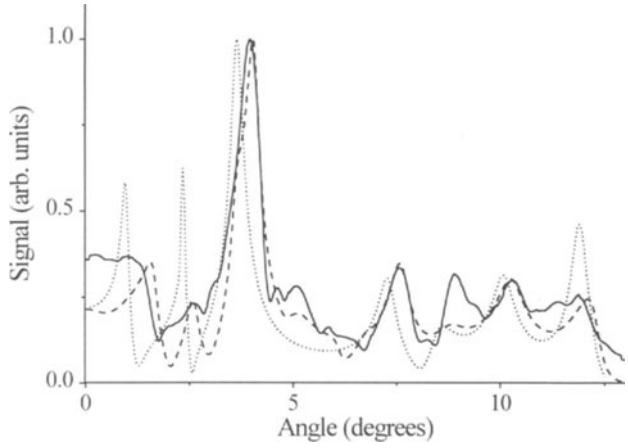

Figure 6. Experimental (solid curve) and calculated (dashed curve) transmission function $S(\theta)$ and appropriate transmission coefficient $T(\theta)$ for 3.6-mm uniaxial carbon-epoxy laminated plate in the $\phi = 45°$ direction.

Figure 7. Air-coupled C-scan of repaired composite specimen showing damage in the repaired area, a large circular feature transected by prepreg tape borders. The inner circle, showing the bond zone of a tapered repair insert, contains two clear areas showing damage.

An example of an air-coupled C-scan of a repaired composite part containing simulated defects is shown in Fig. 7. This was performed on a 5.8-mm sample of multiaxial graphite-epoxy at 0.5M MHz with an incident angle of 7°. Several features can be discerned. The repaired area is a large circular feature transected by the prepreg tape borders. The inner circle, showing the bond zone of a tapered repair insert, contains two clear areas (light grayscale) showing damage. These correlate very well with the sample fabrication drawings and with water-coupled scans.

ACKNOWLEDGEMENTS

This paper is based on work in the FAA Center for Aviation Systems Reliability at Iowa State University and supported by the FAA Technical Center, Atlantic City, New Jersey, under Grant number 94G011. We thank D. Schindel for kindly making his foil transducers available on a research basis.

REFERENCES

1. B. T. Khuri-Yakub, J. H. Kim, C.-H. Chou, P. Parent, and G. S. Kino, in *IEEE Ultrasonics Symposium Proc* (Ed B. R. McAvoy) (IEEE, New York, 1988), 503-06.
2. K. Suzuki, K. Huguchi, and H. Tanigawa, IEEE Trans. Ultrason. Ferro. Freq. Contr. 36, 620-27 (1989).
3. W. D. Wright, D. W. Schindel, D. A. Hutchins, J. Acoust. Soc. Am. 95, 2567-75 (1994).
4. M. J. Anderson, J. A. Hill, C. M. Fortunko, N. S. Dogan, and R. D. Moore, J. Acoust. Soc. Am. 97, 262-72 (1995).
5. G. Hayward, J. Bennet, and R. Hamilton, J. Acoust. Soc. Am. 97, 262-72 (1995).
6. M. I. Haller and B. T. Khuri-Yakub, Rev. Sci. Instr. 65, 2095-8 (1994).
7. B. Hosten, D. W. Schindel, and D. A. Hutchins, J. Acoust. Soc. Am. 99, 2116-23 (1996).
8. A. Safaeinili, O. I. Lobkis, and D. E. Chimenti, IEEE Trans. Ultras. Ferroelect. Freq. Contr. 43, 1171-1180 (1996).
9. O. I. Lobkis, A. Safaeinili, and D. E. Chimenti, J. Acoust. Soc. Am. 99, 2727-36 (1996).